



Pergamon

Available online at www.sciencedirect.com

SCIENCE @ DIRECT®

Acta Materialia 51 (2003) 6123–6137



www.actamat-journals.com

An evaluation of switching criteria for ferroelectrics under stress and electric field

J. Shieh, J.E. Huber, N.A. Fleck *

Department of Engineering, Cambridge University, Trumpington Street, Cambridge CB2 1PZ, UK

Received 9 July 2003; received in revised form 9 July 2003; accepted 28 July 2003

Abstract

The multi-axial responses of barium titanate (BaTiO_3) and hard lead zirconate titanate (PZT-4D) are measured for stress and electric field loadings, and are compared to the response of soft lead zirconate titanate (PZT-5H) taken from a previous study. First, poled ferroelectric specimens are subjected to an electric field at an angle to the original poling direction. Second, unpoled ferroelectric specimens are loaded by a uniaxial compressive stress and a parallel, proportional electric field. The switching surfaces of BaTiO_3 and PZT-4D are constructed from the experimental measurements, and compared with existing data for PZT-5H. The measured responses are then used to evaluate the accuracy of existing micromechanical and phenomenological models of ferroelectric switching.

© 2003 Acta Materialia Inc. Published by Elsevier Ltd. All rights reserved.

Keywords: Electroceramics; Ferroelectricity; Micromechanical modelling

1. Introduction

Ferroelectric polycrystals exhibit a wide variety of coupled electrical and mechanical phenomena, and have been commonly employed in applications such as sensors and actuators. Typically, ferroelectric devices possess complex shapes, with field intensifiers such as embedded electrodes and cracks. A knowledge of the material response in uniaxial loading is essential for the basic design of transducers, whilst a detailed knowledge of multi-axial behaviour is desirable in order to predict

device performance and durability. In broad terms, ferroelectric sensors operate within the linear regime with subsequent signal amplification: linearity is more important than signal power. In other applications such as ferroelectric actuators, non-linear behaviour is a consequence of operating at high power.

It is useful to introduce the concept of a *switching surface* for a ferroelectric material. The switching surface is the locus of points in combined electric field (E) and stress (σ) space, within which the material displays no ferroelectric switching. It is analogous to the initial yield surface in conventional plasticity theory, and the same caveats apply: at room temperature, creep becomes significant on a time scale of minutes and longer.

* Corresponding author. Tel.: +44-1223-332781; fax: +44-1223-332662.

E-mail address: naf1@eng.cam.ac.uk (N.A. Fleck).

The existing literature on the electro-mechanical performance of ferroelectrics has concentrated upon the measurement of the uniaxial response [1,2]. These studies have demonstrated that poled ferroelectrics are anisotropic, and exhibit hysteresis in strain and electric displacement, memory effects, rate effects and strong electro-mechanical coupling. For example, Cao and Evans [1] performed uniaxial compression tests on hard and soft PZT ceramics; they found that electrically poled hard PZT can sustain appreciable stress (up to 200 MPa) without significant depoling, whereas poled soft PZT is susceptible to depoling at stresses on the order of 50 MPa. Lynch [2] performed a compressive test on poled PLZT 8/65/35, and by measuring the electric displacement response in addition to strain, showed that depolarization begins at the remarkably low stress level of 5 MPa.

The current study has two aims: (i) to present a family of measured responses for a range of ferroelectric solids, and (ii) to describe the main elements of ferroelectric behaviour which switching models should capture. The outline of the paper is as follows. *First*, recent models for ferroelectric behaviour are reviewed. Switching criteria for both micromechanical and phenomenological models are summarised, and the resulting switching surfaces are compared. *Second*, an experimental investigation into the switching behaviours of barium titanate (BaTiO_3) and hard lead zirconate titanate (PZT-4D) is reported. Two types of multi-axial testing are performed: (i) poled specimens are subjected to an electric field at an angle to the original poling direction, and (ii) unpoled specimens are loaded by a uniaxial compressive stress and a parallel, proportional electric field. The first type of test involves non-proportional loading and causes rotation of the polarization vector. The second type of test explores the sensitivity of switching to the relative magnitude of mechanical and electrical loading. *Third*, the measured responses of BaTiO_3 and PZT-4D, together with previous measurements on PZT-5H [3,4], are used to assess the accuracy of existing micromechanical and phenomenological switching models.

2. Review of multi-axial models for ferroelectrics

At present no model is capable of predicting the full range of responses of soft and hard ferroelectrics under general electro-mechanical loading; however, substantial progress has been made in predicting the response to combined uniaxial stress and electric field. Existing multi-axial models of ferroelectric behaviour fall into two classes—micromechanical and phenomenological; these are reviewed in turn.

2.1. Micromechanical models

Micromechanical models are based on a description of the material at the domain or single crystal length scale, and make use of homogenization theory to reproduce polycrystal behaviour (see [5–10]). These models range in complexity of homogenization scheme from simple Reuss averages (e.g. [5]) to self-consistent estimates (e.g. [10]). Hwang and co-workers [5] used a hysteresis model to predict the non-linear response of each ferroelectric grain to the imposed electric field and stress. The model assumes that each grain contains a single domain, with the macroscopic response given by volume averaging the response of each randomly oriented grain. The switching criterion for each grain is:

$$E_i \Delta P_i + \sigma_{jk} \Delta \varepsilon_{jk} \geq 2P_0 E_0 \quad (1)$$

where ΔP and $\Delta \varepsilon$ are the changes in spontaneous polarization and spontaneous strain, respectively. P_0 and E_0 are the magnitudes of the spontaneous polarization and critical electric field for switching, respectively. The quantity $2P_0 E_0$ is the work done per unit volume in transforming material between any two polarization states. The resulting switching surfaces of a single tetragonal ferroelectric crystal in electric field space (E_3 – E_1) and in electric field-stress space (E_3 – σ_{33}) are illustrated in Fig. 1. Here, the principal directions of loading are aligned with the material axes. The switching surface for the single grain is shown as a solid line, and is the inner envelope of the surfaces defined by (1) for all possible switches (shown as dashed lines in Fig. 1a). The labels in parentheses for each switching

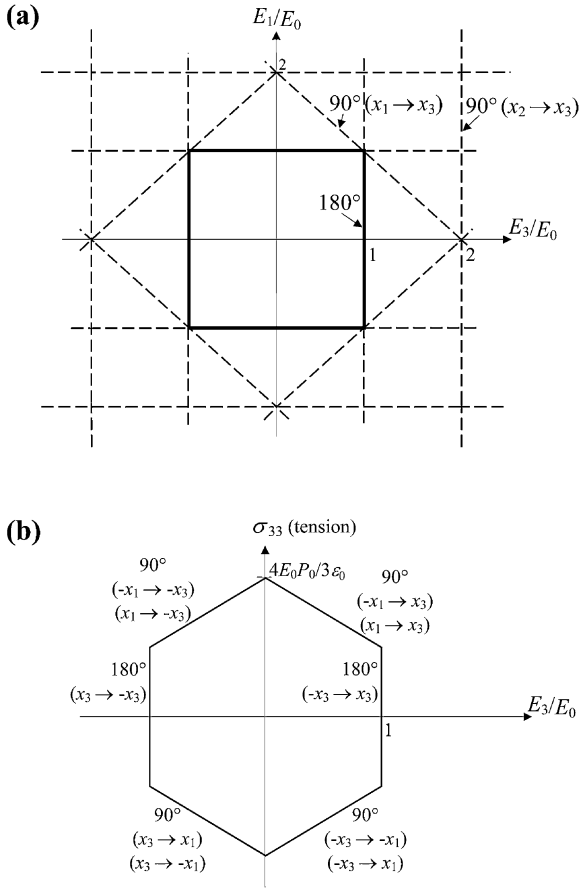


Fig. 1. (a) Switching surface of a single tetragonal ferroelectric crystal in electric field (E_3, E_1) space, based on the switching criterion of Hwang et al. [5]. (b) Switching surface of a single tetragonal ferroelectric crystal in electric field-stress (E_3, σ_{33}) space, based on the switching criterion of Hwang et al. [5] (Labels such as $(x_1 \rightarrow x_3)$ denote a domain with an initial polarization in the x_1 direction switching to align with the x_3 direction.)

line indicate the initial and final direction x_i of polarization for each domain. Note that there is no change in spontaneous strain for 180° switching and consequently 180° switching is not activated by stress: the term $\sigma_{ij}\Delta\epsilon_{jk}$ in (1) vanishes.

McMeeking, Hwang and co-workers [6,7] and Chen and Lynch [8] extended the model of Hwang et al. [5] to include the effects of a back-stress and a back-electric field. They argued that each ferroelectric grain is constrained electrically and mechanically by the neighbouring grains. The difference

between local stress and electric fields within each grain and the remotely applied fields defines the back-field, and can be sufficiently large to give a reversal of switching during unloading. Hwang et al. [7] assumed that each ferroelectric grain comprises a single domain; they treated each grain as a linear piezoelectric spherical inclusion following Eshelby's method. The switching criterion for each grain was obtained as [6–8]:

$$\alpha \left(\sigma_{ij} + \frac{2}{5} \bar{Y} \epsilon_{ij}^{rm} \right) \Delta \epsilon_{ij}^{ri} + \left(E_i + \frac{1}{3\kappa} P_i^{rm} \right) \Delta P_i^{ri} \geq 2 \bar{E}_0 P_0 \quad (2)$$

where α is a parameter which weights the mechanical and electrical terms, ϵ^{rm} and P^{rm} are the current values of remanent strain and remanent polarization of the ferroelectric matrix with a fixed dielectric permittivity κ and fixed modulus \bar{Y} , $\Delta \epsilon^{ri}$ and ΔP^{ri} are the changes in spontaneous strain and spontaneous polarization of a spherical piezoelectric inclusion due to switching, and \bar{E}_0 is the effective coercive field magnitude for switching. Chen and Lynch [8] embellished the model of Hwang et al. [7] to include saturation of the piezoelectric effect at high field levels.

Kessler and Balke [9] have argued that switching occurs at a material point when the drop in free energy upon switching attains a critical value. On writing (E_b, σ_b) and (E_a, σ_a) as the electric field and stress before and after switching, they derived the following point-wise switching criterion:

$$\frac{E_b + E_a}{2} \Delta P^r + \frac{\sigma_b + \sigma_a}{2} \Delta \epsilon^r + \frac{E_b E_a}{2} \Delta \kappa + \frac{\sigma_b \sigma_a}{2} \Delta S + \frac{E_b \sigma_a + E_a \sigma_b}{2} \Delta d \geq 2 P_0 E_0 \quad (3)$$

where $\Delta \kappa$, ΔS and Δd are the assumed values of finite jump in dielectric permittivity, elastic compliance and piezoelectric coupling tensor upon switching, respectively, and ΔP^r and $\Delta \epsilon^r$ are the jump in remanent polarization and remanent strain upon switching. Kessler and Balke [9] also developed the elementary bounds (Reuss and Voigt) for an isotropic distribution of crystallites.

Huber et al. [10] have developed a micromechanical model which adopts an incremental self-

consistent crystal plasticity scheme to address ferroelectric switching. An analogy was drawn between the slip systems of dislocation plasticity in metals and transformation plasticity by domain wall motion in ferroelectrics. The model of Huber et al. [10] adopts the following switching criterion for each grain:

$$[\sigma \ E] \begin{bmatrix} \Delta \varepsilon_{\alpha}^r \\ \Delta P_{\alpha}^r \end{bmatrix} + \frac{1}{2} [\sigma \ E] \begin{bmatrix} \Delta S_{\alpha} & \Delta d_{\alpha} \\ \Delta d_{\alpha} & \Delta \kappa_{\alpha} \end{bmatrix} \begin{bmatrix} \sigma \\ E \end{bmatrix} \geq 2P_0 E_0 \quad (4)$$

where the subscript ‘ α ’ indicates each potentially active transformation system. Note that switching criteria (3) and (4) become identical for an incremental switch with $E_b = E_a = E$ and $\sigma_b = \sigma_a = \sigma$ in (3).

2.2. Phenomenological models

Phenomenological models are commonly derived from a thermodynamic framework and use fitting functions based on experimental observation (see [3,11–16]). In most phenomenological models, the ferroelectric constitutive law is derived from a postulated Helmholtz free energy statement, with the remanent strain and remanent polarization as internal state variables to capture history dependence. The coefficients of the thermodynamic energy function are calibrated by experiment, and the resulting phenomenological models are well-suited to finite element implementation since they are computationally less intensive than micromechanical models. All phenomenological models and their switching criteria discussed in this section are for polycrystals.

Cocks and McMeeking [13] have developed a phenomenological switching model in a uniaxial form. Their constitutive law is similar to the J2 flow theory version of plasticity with kinematic hardening: a convex switching surface is identified in stress/electric field space within which the response is linear piezoelectric. When the loading point lies on the switching surface, the increments of remanent strain and remanent polarization are constrained to lie along the outward normal to the switching surface. Cocks and McMeeking [13] proposed the following description of the switching surface:

$$\sqrt{(E - E^B)^2 + \alpha(\sigma - \sigma^B)^2} - E_0 \leq 0 \quad (5)$$

where α is the material parameter, and E^B and σ^B are the back-fields derived from a Helmholtz free energy Ψ .

Kamlah and Tsakmakis [14], in common with Bassiouny et al. [11] and Bassiouny and Maugin [12], adopted a rectangular switching surface in stress and electric field space. Thus, they treated the ferroelectric and ferroelastic phenomena as independent, and proposed the following switching surfaces for uniaxial electro-mechanical loading [14]:

$$\text{Ferroelectric: } \sqrt{(E - C^p P^r)(E - C^p P^r)} - E_0 \leq 0 \quad (6)$$

$$\text{Ferroelastic: } \sqrt{(\sigma - C^f \varepsilon^r)(\sigma - C^f \varepsilon^r)} - \sigma_0 \leq 0 \quad (7)$$

where C^p and C^f are material constants. Here P^r is the remanent polarization and ε^r is the remanent strain of the polycrystal. Note that the back-fields are in the form of $E^B = C^p P^r$ and $\sigma^B = C^f \varepsilon^r$.

Huber and Fleck [3], Landis and McMeeking [15] and Landis [16] introduced cross-coupling into the switching function to account for the generation of remanent strain by the application of electric field, and remanent polarization by stress. They each assumed the following switching surface:

$$\sqrt{\hat{E}_i \hat{E}_i + \frac{3\alpha}{2} \hat{s}_{ij} \hat{s}_{ij} + \beta \hat{s}_{ij} \hat{E}_i P_j^r} - E_0 \leq 0 \quad (8)$$

where s_{ij} is the stress deviator, with $\hat{E}_i = E_i - E_i^B$ and $\hat{s}_{ij} = s_{ij} - s_{ij}^B$ (the superscript ‘B’ denotes a back-field). The material parameters α and β are determined by matching the model to the observed material response.

2.3. Comparison of the switching surfaces of the micromechanical and phenomenological models

The switching criteria reviewed above for the micromechanical and phenomenological models are now compared. Consider first the case of purely electrical loading (E_3, E_1) with the component E_2 equal to zero. The predicted switching surface for an initially unpoled isotropic ferroelectric is

sketched in Fig. 2a: all models considered above predict a circular switching surface with radius $|E| = E_0$. However, the models give dramatically different responses for a polycrystal of tetragonal grains which has been initially poled along the positive E_3 direction, see Fig. 2b. (A uniform distribution of grain orientations is assumed in order for the polycrystal to be isotropic in the unpoled state.)

The micromechanical model of Hwang et al. [5] has been used to calculate the switching surface after full saturation of switching along the E_3 —axis. In this limit the surface is unique, independent of any additional material parameters. Calculations of self-consistent behaviour were made using the model of Huber et al. [10] and the prediction for the switching surface after poling to $2E_0$ is taken directly from Fig. 8a of Ref. [10]. The reader is

referred to the previous paper in order to extract the values of material parameters assumed in the model, such as the piezoelectric coefficients and remanent strain of a domain. The self-consistent model has been re-run for poling to $8E_0$, assuming the same set of material parameters, and this prediction is included in Fig. 2b. It is expected that the self-consistent model of Hwang et al. [7] will lead to similar switching surfaces (not shown).

Next consider the predictions by the phenomenological models after poling to $2E_0$ along the E_3 —axis. In general, the switching surfaces after poling are elliptical in shape and are shifted along the positive E_3 —axis. For the purposes of the present discussion, the switching surface is plotted for the simplest case of a solid with uncoupled electrical and mechanical fields, as specified by (6). For this case, a circular switching surface is obtained, centred at $E^B = E_0$ and with a radius of E_0 in E_3 — E_1 space.

The phenomenological models give a smooth switching surface while the self-consistent models predict the emergence of a vertex at the loading point; these features mirror those of conventional plasticity theory (see [17]). In general the models predict that the switching surfaces are closed, for any finite value of poling field. The exception is the fully switched locus of Hwang et al. [5]; this corresponds to an infinite value of poling field E_3 , and results in an open switching surface.

Now consider the case of combined loading by a uniaxial stress σ_{33} and a co-directional electric field E_3 . The predicted switching surface in (E_3, σ_{33}) space for an initially unpoled isotropic ferroelectric is shown in Fig. 3. All models have sufficient flexibility for the uniaxial yield strength σ_0 in the unpoled state to be specified independently of the coercive field strength E_0 . As discussed above, the phenomenological model of Kamlah and Tsakmakis [14] assumes uncoupled behaviour so that the switching surface is rectangular in (E_3, σ_{33}) space. In contrast, the other phenomenological models and the self-consistent models of Huber et al. [10] and Hwang et al. [5,7] give a coupled response. Several phenomenological models [3,13–16] assume an elliptical switching surface in (E_3, σ_{33}) space, see Eq. (8). The switching locus for the self-consistent model of Huber et al. [10] is

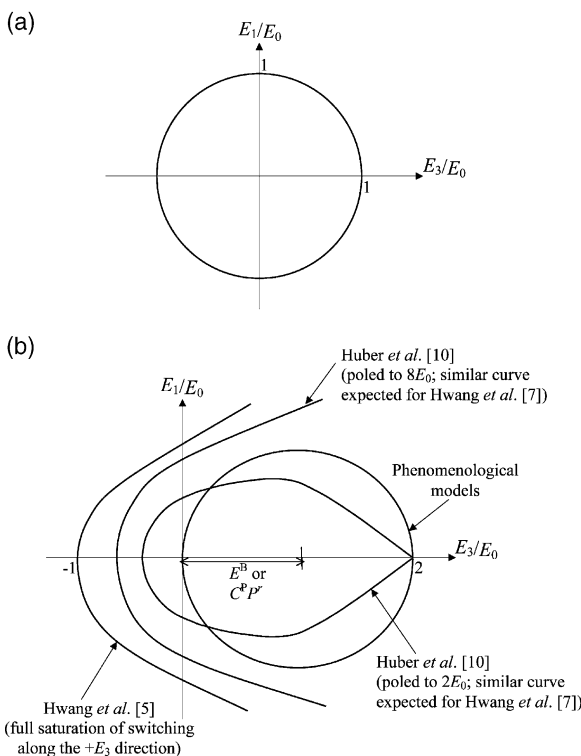


Fig. 2. (a) Switching criteria introduced or assumed by various models for an unpoled tetragonal polycrystal in (E_3, E_1) space. (b) Switching criteria introduced or assumed by various models for an E_3 -direction poled tetragonal polycrystal in (E_3, E_1) space.

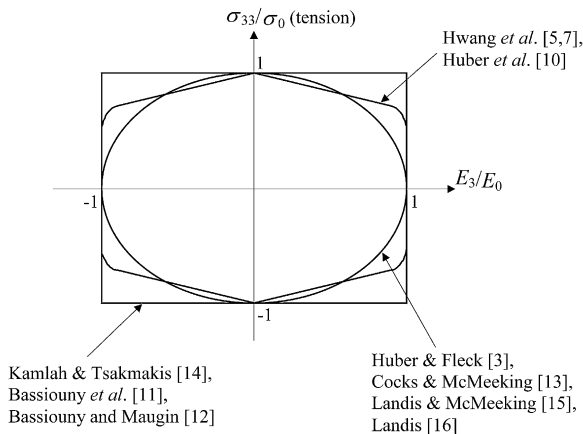


Fig. 3. Switching criteria introduced or assumed by various models for an unpoled tetragonal polycrystal in (E_3, σ_{33}) space.

dependent upon a number of material parameters, and these are detailed in Huber and Fleck [18]. It is concluded from Fig. 3 that the various models give a spread in qualitative behaviour, and this motivates a set of critical experiments to assess the accuracy of the models.

There exists a lack of comprehensive experimental data in combined electro-mechanical loading, against which models can be validated. In the following sections, measured multi-axial responses of BaTiO₃ and of the hard PZT material PZT-4D to stress and electric field loading are reported. In order to give a more complete picture, these responses are compared with that of soft PZT-5H, taken from [3,4].

3. Experimental procedure

3.1. Choice of materials

Two polycrystalline bulk ferroelectric ceramics were used in this study: BaTiO₃ and PZT-4D. Polycrystalline BaTiO₃ of grain size 3–12 μm in the tetragonal phase was supplied in bulk form.¹ It has a Curie temperature of approximately 130 °C. Polycrystalline PZT-4D of grain size 5–10 μm was

supplied by Morgan Matroc Ltd.² It is classified as a “hard” ceramic, and has a Curie temperature of approximately 320 °C. Both the BaTiO₃ and PZT-4D materials were thermally depoled to an isotropic state.

3.2. Preliminary measurements

Preliminary tests were carried out on BaTiO₃ and PZT-4D materials to measure the coercive field strength E_c , remanent polarization P_r after poling at room temperature, and to select maximum load levels σ_{max} and E_{max} for all subsequent polarization rotation and proportional loading tests.

Cuboidal specimens measuring 5 mm × 5 mm × 3 mm for BaTiO₃ and 5 mm × 5 mm × 2 mm for PZT-4D were cut from the unpoled isotropic bulk materials. The thinner 2 mm specimens of PZT-4D were needed to allow high electric field strengths at a practical working voltage. Conductive silver paint was used to produce electrodes on each 5 mm × 5 mm surface. Each specimen was mounted in a loading fixture as shown in Fig. 4. The loading fixture consisted of brass plates, providing electrical contact to the electrode surfaces of the specimen, nylon spacers to insulate the specimen from the load frame, and a steel spherical alignment fixture to accommodate slight misalignment of the specimen. The upper brass plate was connected to ground via a 2.96 μF metering capacitor; the voltage across this capacitor was used to measure charge accumulation on the specimen electrodes. The lower brass plate was connected to the high voltage output of a Trek 20/20C amplifier. The entire loading fixture was supported in a silicon oil bath to prevent breakdown arcing, and forces were applied using an Instron 5500R test frame. All tests were carried out at temperatures in the range of 17–21 °C.

To measure E_c , a low frequency (0.2 Hz) cyclic electric field was applied to a specimen of each material with gradually increasing amplitude. When the amplitude was sufficient to produce a

¹ AWE Aldermaston, Reading, Berkshire RG7 4PR, UK.

² Morgan Matroc Ltd., Transducer Products Division, Thornhill, Southampton SO9 5QF, UK.

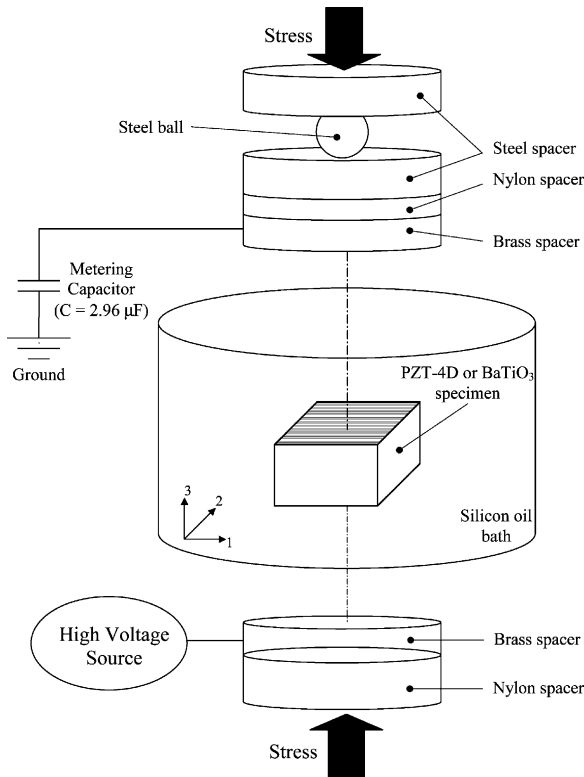


Fig. 4. Schematic of the electro-mechanical loading system.

dielectric hysteresis D – E curve showing ferroelectric switching and saturation, the load amplitude was held constant for several complete cycles and the stable D – E curve was recorded, see Fig. 5. The coercive field values were read directly from the D – E curve for each material. For the purposes of comparison, the D – E curve for PZT-5H is included in Fig. 5. The peak field to produce full hysteresis D – E curves was chosen as E_{\max} , with the chosen values listed in Table 1. The maximum electric field loading level E_{\max} was chosen to be at least twice the coercive field, and sufficiently high to obtain a substantial saturation of polarization. (Complete saturation could not be achieved at practical loading levels.)

To measure P_r , a single half cycle triangular wave of electrical loading was applied to a new specimen of each material, with electric field rising steadily from zero to E_{\max} , followed by the electric field returning steadily to zero. The specimens were “poled” by this procedure, and the remanent

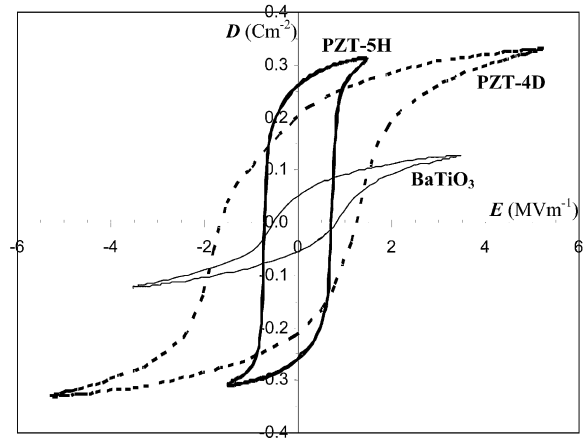


Fig. 5. Measured dielectric hysteresis curves (electric displacement D versus electric field E) for BaTiO₃, PZT-4D and PZT-5H ($f_{\text{app}} = 0.2$ Hz).

Table 1
Preliminary measurements and selections on BaTiO₃, PZT-4D and PZT-5H

Material	Coercive field E_c (MV m ⁻¹)	Selected saturation field E_{\max} (MV m ⁻¹)	Remanent polarization P_r (C m ⁻²)	Selected depoling stress σ_{\max} (MPa)
BaTiO ₃	0.65	3.25	0.055	400
PZT-4D	1.4	5.0	0.165	500
PZT-5H	0.7	1.5	0.260	300

polarization values of the two materials after poling were read directly from the metering capacitor. Note that the measured values of P_r are affected by the maximum applied electric field E_{\max} ; however, since E_{\max} was chosen so as to produce substantial saturation, the P_r values are only weakly sensitive to the choice of E_{\max} . The poled specimen of each material was subsequently loaded in uniaxial compression parallel to the poling direction—the chosen value of maximum stress σ_{\max} was sufficient to produce substantial depolarization of the poled specimen, for each material. Complete depolarization could not be achieved at σ_{\max} since the chosen σ_{\max} for each material must be less than its failure stress in compression. The chosen values of σ_{\max} for each material are also listed in Table 1, along with the

measured values of E_c and P_r . Similar data for PZT-5H, taken from [3,4], are included in Table 1.

3.3. Polarization rotation test

Plates of dimension $25\text{ mm} \times 25\text{ mm} \times 5\text{ mm}$ were cut from the unpoled isotropic bulk BaTiO_3 and PZT-4D materials using a diamond saw. Conducting surface electrodes were made on the $25\text{ mm} \times 25\text{ mm}$ faces by painting with a thin layer of silver electrode paint. The plates were then poled by applying electric fields through the plate thickness of magnitude E_{max} at room temperature for 40 s. After poling, the surface electrodes of the plates were removed by light polishing. The plates were then cut using a diamond saw into cuboidal blocks, with the faces of the blocks cut at differing angles θ_c to the direction of remanent polarization, as shown in Fig. 6. A family of cuboidal specimens with face normals inclined at $\theta = 0^\circ, 30^\circ, 60^\circ, 90^\circ, 120^\circ, 150^\circ$ and 180° to the poling direction (i.e. the direction of remanent polarization) were produced. Depending on the angle of cut, the resulting cuboidal specimens varied in size from $5\text{ mm} \times 5\text{ mm} \times 1.5\text{ mm}$ (cut at $\theta_c = 0^\circ, 90^\circ$ and 180°) to $5\text{ mm} \times 3.5\text{ mm} \times 1.5\text{ mm}$ (cut at $\theta_c = 30^\circ, 60^\circ, 120^\circ$ and 150°). All specimens were lightly polished with 2500 grit SiC paper and electroded by painting with silver electrode paint to allow an electric field to be applied at angles of 0° – 180° to the direction of remanent polarization, in steps of 30° .

The loading arrangement and loading paths for

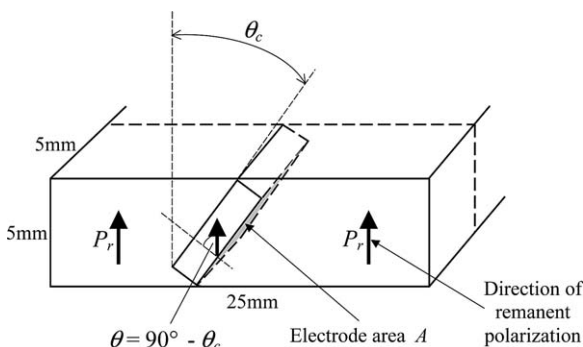


Fig. 6. Cutting out of a block of poled material at angle θ_c .

the polarization rotation test are shown in Fig. 7. The Trek 20/20C high-voltage amplifier supplied the electric field loading, and the electric charge at the specimen's surface electrodes was measured by the voltage across a $2.96\text{ }\mu\text{F}$ metering capacitor connected in series with the specimen and placed between the specimen and ground. The original poling operation for each specimen corresponds to loading along path OA (see Fig. 7b) followed by unloading. A half-cycle triangular wave of electrical loading was then applied to each specimen by following one of the loading paths OA to OG ; in each case the electric field was increased from zero to E_{max} and back to zero, over a period of about 30 s. The applied voltage and the surface charge on the electrodes were recorded throughout. All tests were carried out at a temperature in the range

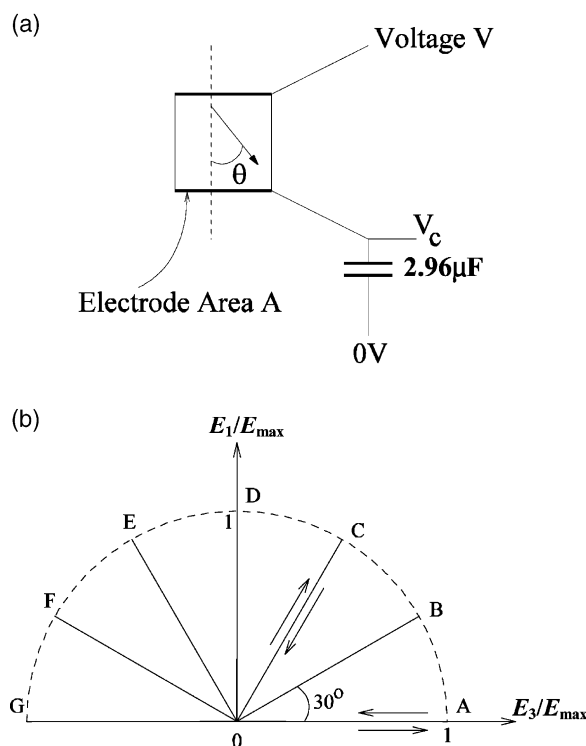


Fig. 7. (a) General arrangement for multi-axial electrical loading—electric field is applied at angle θ to the original poling direction. (b) Loading paths for multi-axial electrical loading—specimens are first loaded (poled) along path OA followed by unloading, and then re-loaded along different paths, OA to OG , followed by unloading.

of 17–21 °C, with the specimen contained within a silicon oil bath to prevent electrical breakdown.

3.4. Proportional loading test

Cuboidal specimens measuring 5 mm × 5 mm × 3 mm for BaTiO₃ and 5 mm × 5 mm × 2 mm for PZT-4D were cut from the unpoled isotropic bulk materials. The specimens were lightly polished with 2500 grit SiC paper and conducting surface electrodes were made on the 5 mm × 5 mm faces by painting with a thin layer of silver electrode paint. Each specimen was then mounted in a loading fixture identical to the one used in the preliminary tests (see Section 3.2 for details). A 10 kN load cell was used to measure the force carried by the specimen. The speed of the test frame cross-head was set to 5 × 10⁻³ mms⁻¹.

The load cell output of the test frame was connected by a variable gain amplifier and low pass filter to the input of the Trek 20/20C high-voltage amplifier. Electrical loading of the specimen was thus driven by the mechanical load measurement, such that the electric field supplied by the high-voltage source was directly proportional to the uniaxial compressive stress (see Fig. 8a). By adjusting the amplifier gain for different specimens it was possible to follow the loading paths OA to OG of Fig. 8b, with the combined electrical and mechanical loading following an approximately triangular waveform, rising to its peak value and falling steadily to zero over about 30 s. In each loading case, the peak applied load (E_3, σ_{33}) was set to ($E_{\max}\cos\theta, \sigma_{\max}\sin\theta$) where θ took the values 0°, 15°, 30°, 45°, 60°, 75° and 90° for tests OA to OG, respectively. Thus, the specimen experienced purely electrical loading when $\theta = 0^\circ$, and purely mechanical loading when $\theta = 90^\circ$. (For the case of $\theta = 0^\circ$, the purely electrical loading supplied by the high-voltage source was driven by a signal generator, and not by the mechanical load measurement.) The ratio of stress to electric field σ_{33}/E_3 remained constant throughout each test, to within 0.5%. Throughout the test, the applied electrical and mechanical loads and the surface charge on the electrodes were recorded continuously.

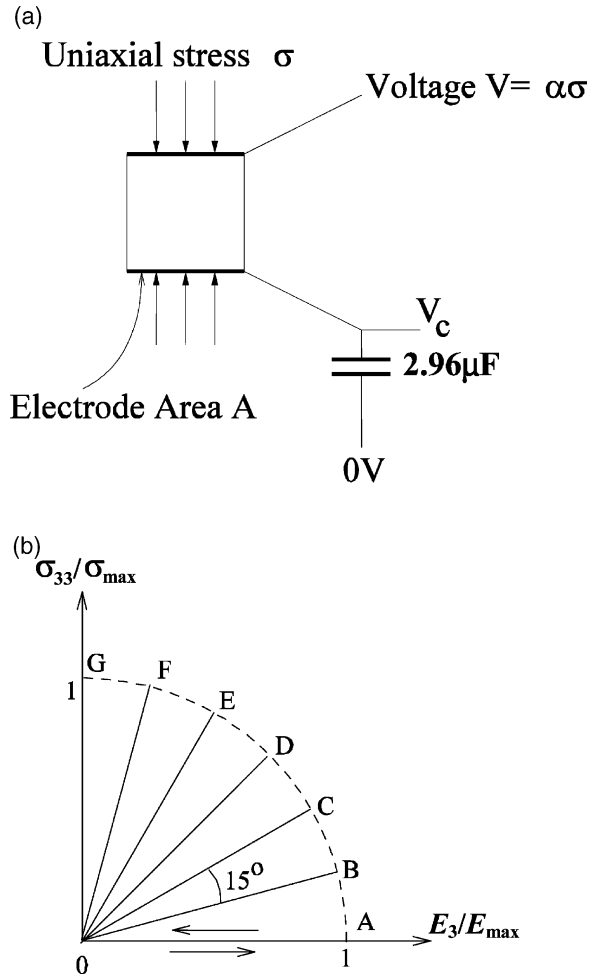


Fig. 8. (a) General arrangement for proportional electro-mechanical loading with uniaxial stress σ and electric field E ; the specimen is initially unpoled. (b) Loading paths for proportional electro-mechanical loading with uniaxial stress σ and electric field E —initially unpoled specimens are loaded along one of the paths OA to OG and unloaded.

4. Observations and test measurements

4.1. Polarization rotation test

The poled BaTiO₃ and PZT-4D were re-loaded by an electric field at an angle θ to the original poling direction, resulting in ferroelectric switching. The measured D – E responses to the polarization rotation test are shown in Fig. 9a for BaTiO₃ and in Fig. 9b for PZT-4D. Similar measurements

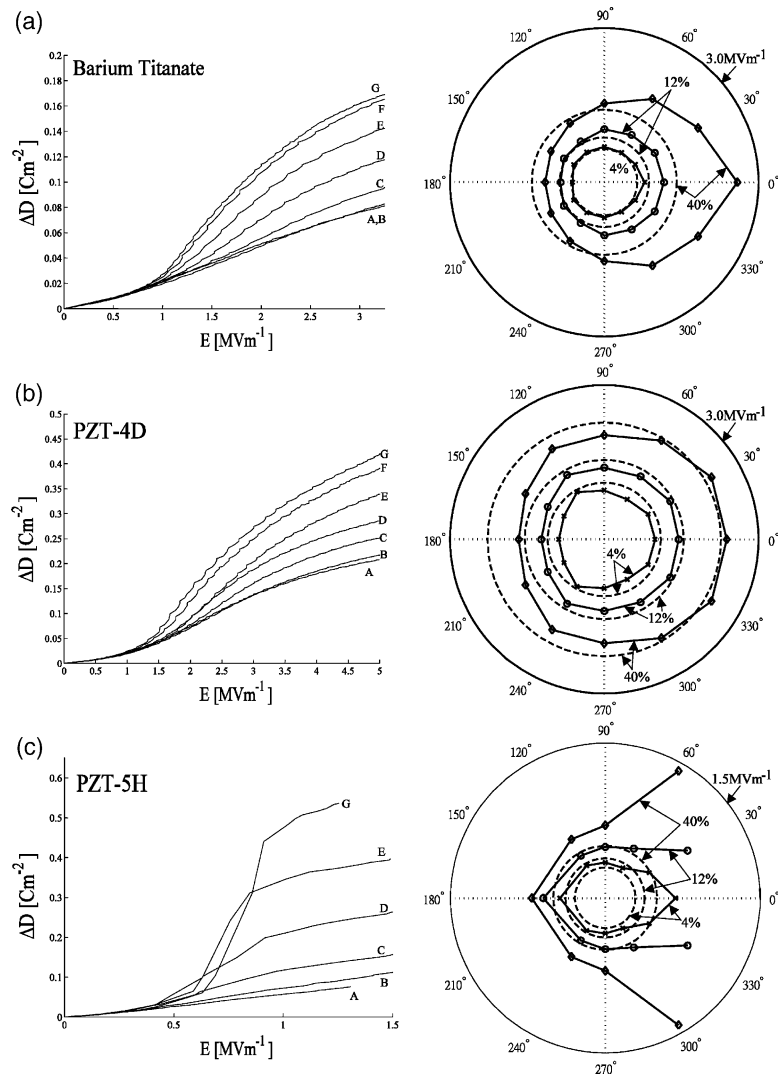


Fig. 9. Measured responses to a polarization rotation test for three materials: (a) BaTiO₃, (b) PZT-4D and (c) PZT-5H. For each material, the left-hand side figure shows the change in electric displacement ΔD versus electric field E response of specimens loaded along paths OA to OG shown in Fig. 7b (i.e. inclined at various angles θ to the initial poling direction OA), while the right-hand side figure shows the corresponding offset switching surfaces (solid curves) for three levels of offset corresponding to 4%, 12% and 40% of the remanent polarization after cold poling, with the radial axis showing electric field in MV m⁻¹ and the polar axis showing angle θ . In contrast, the dashed circles shown in the right-hand side figure for each material are the unpoled (isotropic) switching surfaces corresponding to the same levels of remanent polarization offset.

on PZT-5H (taken from [3]) are also shown in Fig. 9c. Only the re-loading curves are shown in the figure, with the subsequent unloading responses omitted for clarity. The curves A to G correspond to the loading paths OA to OG in Fig. 7b. The 0° specimen (denoted 'A' for path OA) represents the

case where the applied electric field is in the same direction as the remanent polarization. Since the measured D – E hysteresis curves (see Fig. 5) for BaTiO₃ and PZT-4D showed a significant reversal of switching during unloading, it is concluded that switching was not saturated after the original

poling process, and consequently, re-loading the 0° specimen along path OA gave rise to ferroelectric switching. In contrast, the 0° specimen ('A') for PZT-5H behaved in an approximately linear response, indicating that switching was saturated during poling, and remained saturated during unloading. The 180° specimen ('G') represents the case where the applied field is parallel to the remanent polarization, but in the opposite direction. In all three materials, loading the 180° specimen along OG resulted in polarization reversal, which produced a change in electric displacement of approximately $2P_r$.

The measured D – E responses suggest that as the angle between the loading direction and the direction of remanent polarization is increased, the overall change in electric displacement increases accordingly. It is evident that the responses of BaTiO₃ and PZT-4D are similar in shape, but differ in the magnitude of coercive field E_c and remanent polarization P_r . In all three materials, the initial slope dD/dE is almost independent of the angle between the loading direction and the original poling direction; thus the dielectric permittivity tensor of each material, measured under quasi-static loading, is close to isotropic, even in the poled state.

For each response A to G , the change in electric displacement with electric field is close to linear under electric field loading of less than $0.3E_c$. For electric field loading greater than $0.3E_c$, non-linear behaviour due to ferroelectric switching is evident. The switching surface in electric field space is constructed from the D – E responses A to G by taking the electric field level at selected values of polarization offset: surfaces for an offset polarization of 4%, 12% and 40% of P_r are shown as solid lines in Fig. 9 in polar form. Note that these offset values are purely arbitrary measures of the extent of switching. The electric field values taken from responses A to G form the upper half ($0^\circ \leq \theta \leq 180^\circ$) of the 4%, 12% and 40% switching surfaces shown in Fig. 9. The lower half of each switching surface is inferred from symmetry. Dashed circles in Fig. 9 show the 4%, 12% and 40% switching surfaces for each material in the unpoled (isotropic) state. These are included for later comparison between the poled and unpoled states.

4.2. Proportional loading test

The responses of initially unpoled BaTiO₃ and PZT-4D to the proportional, combined loading of uniaxial compressive stress and electric field are shown in Fig. 10. For each solid, the electric displacement D_3 is plotted against the electric field E_3 and against the compressive stress σ_{33} . A total of seven loading paths A – G were considered, as sketched in Fig. 8b. Note that the response G corresponds to stress loading (i.e. path OG) of an unpoled, isotropic specimen. Symmetry dictates that no electric displacement is generated in an unpoled specimen by a mechanical stress, and so this test is not shown in Fig. 10. The responses labelled A to F in Fig. 10 are the results of loading the unpoled specimens along paths OA to OF , respectively. Both the loading and unloading portions of the response are shown in Fig. 10 for each test. Despite the widely differing values of E_c and P_r , the behaviours of BaTiO₃, PZT-4D and PZT-5H are qualitatively similar. In fact, the responses A to F of BaTiO₃ and PZT-4D, appropriately normalised by the values of P_r , E_{\max} and σ_{\max} in Table 1 appear almost identical. The soft PZT-5H differs from PZT-4D and BaTiO₃ in that full switching occurs relatively abruptly when the coercive field strength is reached.

The switching surfaces for unpoled BaTiO₃, PZT-4D and PZT-5H under electro-mechanical loading are shown in Fig. 11. These switching surfaces are constructed as follows: a load parameter L is defined by $L^2 = (E_3/E_{\max})^2 + (\sigma_{33}/\sigma_{\max})^2$, where the saturation field E_{\max} and the depoling stress σ_{\max} are listed in Table 1. The value of L increases from zero to unity at peak load. For the purposes of constructing the switching surface the non-linearity associated with the progressive development of the piezoelectric effect (associated with poling) is neglected. For each response in Fig. 10, the value of L corresponding to the polarization reaching $4\%P_r$ defines a combination of electric field and stress which constitutes a point on the 4% offset switching surface. Using the family of responses A to F , a set of points on the 4% offset switching surface in (E_3 – σ_{33}) space are found, and these are shown in Fig. 11 (marked 'x'). Similarly, 12% and 40% switching surfaces are constructed

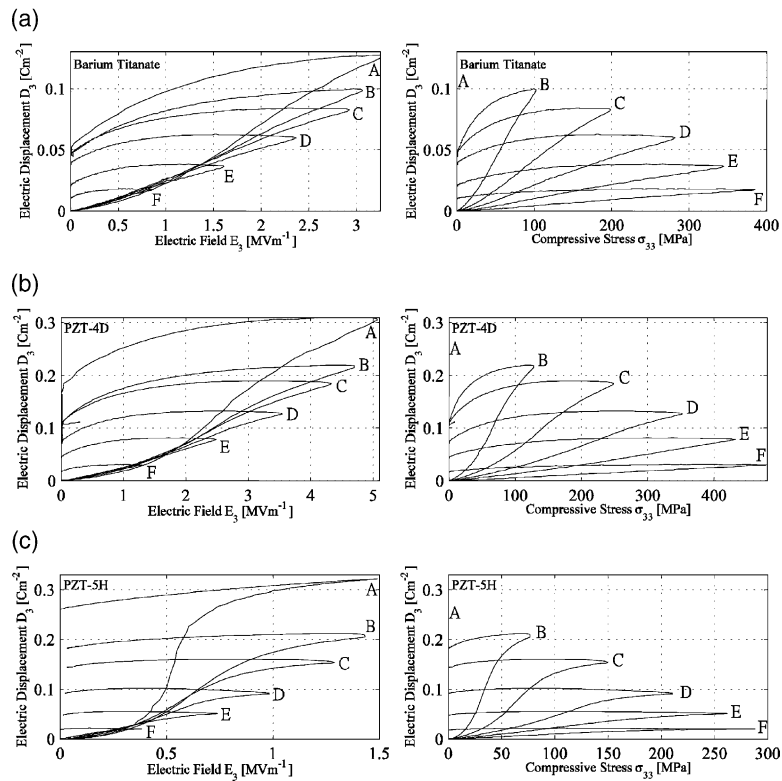


Fig. 10. Measured responses to a proportional loading test with uniaxial stress and electric field for (a) BaTiO₃, (b) PZT-4D and (c) PZT-5H. For each material the electric displacement D_3 versus applied electric field E_3 response, and the same electric displacement measurement D_3 against the corresponding compressive stress σ_{33} are shown. The electric field and stress loads follow the paths OA to OG shown in Fig. 8b.

(marked '○' and '◇', respectively, in Fig. 11). The measured points on the switching surfaces necessarily lie on the loading paths marked as radial, dotted lines in Fig. 11. Proportional loading tests were conducted up to a load intensity of $L = 1$; in several cases, this load intensity level caused insufficient switching to reach the prescribed polarization offset values, hence, no points are recorded on the switching surfaces for these loading conditions. Note that the piezoelectric effect is significant when the ceramics have polarization of 40% P_r and thus the 40% offset switching surfaces are approximate.

5. Discussion

We now compare the measured switching surfaces shown in Figs. 9 and 11 with the switching

surfaces of various models, as shown in Figs. 2b and 3.

5.1. Polarization rotation test

First consider the switching surfaces in electric field space (E_3-E_1), for the poled materials (Fig. 9). In the phenomenological models under discussion, the switching surface assumed for poled material is elliptical in (E_3-E_1) space. This is in good agreement with the measured switching surfaces of BaTiO₃ and PZT-4D and that of PZT-5H with a 4% polarization offset. There is some evidence of vertex formation at the loading point on the switching surface in PZT-5H: this feature is predicted by micromechanical models, but is absent in the phenomenological models.

In several phenomenological models, a stable cyclic hysteresis is achieved by assuming kinem-

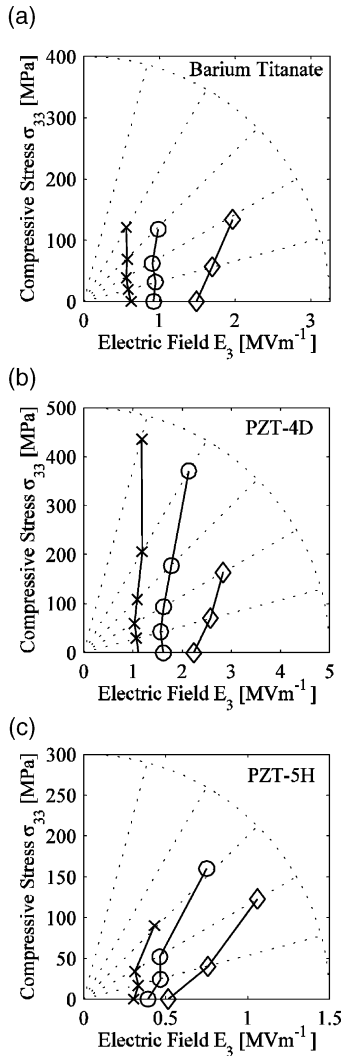


Fig. 11. Offset switching surfaces under proportional loading with uniaxial stress and electric field for (a) BaTiO₃, (b) PZT-4D and (c) PZT-5H, corresponding to the responses shown in Fig. 10. In each case the switching surfaces correspond to offsets of 4% P_r (marked 'x'), 12% P_r (marked 'O') and 40% P_r (marked '◇').

atic hardening within a flow theory. Then, in the absence of isotropic hardening, poling with an electric field E_3 of magnitude $2E_0$ translates the switching surface in (E_3-E_1) space by a distance E_0 . The results in Fig. 9 provide some evidence of a translation of the switching surface. However, the extent of translation is small: the centre of the 4% switching surface remains within $0.2E_c$ of the ori-

gin for all three materials, although they have each been loaded with electric field of magnitude greater than $2E_c$. Note that all measurements were made after unloading from the poled state, and kinematic hardening models allow for return of the switching surface centre towards the origin during unloading of the poling field, provided switching occurs during unloading. It was not practical in the present set of experiments to probe the switching surface in the fully poled state before unloading the poling field.

In both BaTiO₃ and PZT-4D, there is little evidence of isotropic hardening: the field magnitude required to produce switching in the poled state is not substantially different from that needed in the unpoled state. Conversely, in PZT-5H, the electric field magnitude needed for a 12% or 40% offset in polarization is much greater in poled material than in unpoled, for loading with electric field inclined at angles of less than 60° to the poling direction. Here, however, the effect is not isotropic hardening; rather, the switching surface becomes an open locus because of the saturation of switching in the poling direction. Referring to Fig. 10, the curves marked 'A' are the electric displacement response of each material during poling. When PZT-5H is poled, switching reaches almost full saturation in the poling direction and the saturated state remains during unloading: the unloading curve is almost linear. The result is the open switching surfaces seen in Fig. 9c. Open switching surfaces are not seen for BaTiO₃ or PZT-4D because a reversal of ferroelectric switching occurs when the poling field is removed. The reversal is not complete, but it is sufficient to allow further switching when the material is reloaded in the poling direction. The dielectric hysteresis of PZT-4D and BaTiO₃ is similar to the mechanical hysteresis of materials such as filled elastomers, or super-elastic shape memory alloys: there is substantial but incomplete recovery of the original state, after unloading. The variety of behaviour seen in PZT-5H, PZT-4D and BaTiO₃ can be captured in a micromechanical model by varying the set of available switching systems. If switching in each grain is dominated by a small number of switching systems, the behaviour is like that of PZT-4D or BaTiO₃. Conversely, if many systems are present

in each grain, behaviour like that of PZT-5H results. This is discussed further in a separate paper [18].

In all three materials, poling in the $+E_3$ direction has little effect upon the switching surface in the region $E_3 < 0$. Thus the region of the switching surface far from the loading point remains almost unchanged during electric field loading, whilst the region close to the loading point changes shape. The resulting shape change is complex, but can be captured approximately by micromechanical models, where the state of the microstructure is stored in a set of internal variables, corresponding to the set of possible switching systems. In phenomenological models, the subtle changes in shape of the switching surface due to saturation of a subset of the switching systems are difficult to capture; a combination of isotropic and kinematic hardening can be used to approximate the effect.

5.2. Proportional loading test

Next consider the switching surfaces shown in Fig. 11. The surfaces for 4% polarization offset are nearly straight lines, independent of stress. If normality of the remanent strain and polarization increments to the switching surface is assumed, the independence from stress implies an absence of remanent straining. In all three materials, it appears that the initial switching from the isotropic state is by non-straining systems (such as 180° switching), or by straining systems that produce no remanent polarization increment (these would go undetected in our test). This is consistent with the independent switching surfaces assumed by Kamlah and Tsakmakis [14] and others. The switching surfaces of several micromechanical models, shown in Fig. 3, are also in agreement, provided that switching systems that produce both strain and polarization (such as 90° systems) are inactive. Note that remanent strains were not measured in the present set of experiments and further work is needed to characterise the strain and polarization response.

6. Conclusion

This study presents a methodology for assessing multi-axial models of ferroelectric behaviour. Mea-

sured switching surfaces for BaTiO₃, PZT-4D and PZT-5H are compared with those predicted or assumed by various models. Two sets of switching surfaces for each material have been measured. The first set of switching surfaces was for material in the poled state, probed by electric field loading. The second set was for material in the unpoled (isotropic) state, probed by proportional loading with a uniaxial compressive stress and a coaxial electric field. The material responses show similarity in the unpoled state, but there is a variety of behaviour in the poled state, depending on the extent to which poling saturates switching, and the reversal of switching during unloading of the poling field. Because of the variety of observed behaviour, a robust material model needs the flexibility to allow changes in the shape, size and position of the switching surface caused by the saturation of switching and the interaction between grains. Phenomenological models typically approximate these effects through hardening rules within a flow theory. These models offer an attractive simplicity that allows them to be calibrated accurately using measured material responses. However, the full range of behaviour seen in the three materials studied here is not readily captured within a single phenomenological model formulation. In contrast, the micromechanical models have a useful flexibility that arises from modelling the underlying mechanism of switching directly. The differences in behaviour at the microstructural scale that give rise to subtle macroscopic effects are thus readily incorporated. A disadvantage of this approach is the difficulty in accurate calibration of the model. However, in multi-axial applications the micromechanical approach is adequate qualitatively, and with due calibration can capture the response quantitatively.

Acknowledgements

The financial support of the EPSRC is gratefully acknowledged. JEH is supported by the Royal Society under a University Research Fellowship.

References

- [1] Cao H, Evans AG. *J Am Ceram Soc* 1993;76(4):890.
- [2] Lynch CS. *Acta Mater* 1996;44(10):4137.
- [3] Huber JE, Fleck NA. *J Mech Phys Solids* 2001;49:785.
- [4] Huber JE, Shieh J, Fleck NA. *Proc SPIE* 2002;4699:133.
- [5] Hwang SC, Lynch CS, McMeeking RM. *Acta Metall Mater* 1995;43:2073.
- [6] McMeeking RM, Hwang SC. *Ferroelectrics* 1997;200(1-4):151–73.
- [7] Hwang SC, Huber JE, McMeeking RM, Fleck NA. *J Appl Phys* 1998;84:1530.
- [8] Chen W, Lynch CS. *Acta Mater* 1998;46(15):5303.
- [9] Kessler H, Balke H. *J Mech Phys Solids* 2001;49(5):953.
- [10] Huber JE, Fleck NA, Landis CM, McMeeking RM. *J Mech Phys Solids* 1999;47:1663.
- [11] Bassiouny E, Ghaleb AF, Maugin GA. *Int J Engng Sci* 1988;26:1279.
- [12] Bassiouny E, Maugin GA. *Int J Engng Sci* 1989;27:975.
- [13] Cocks ACF, McMeeking RM. *Ferroelectrics* 1999;228:219.
- [14] Kamlah M, Tsakmakis C. *Int J Solids Struct* 1999;36:669.
- [15] Landis CM, McMeeking RM. *J Intelligent Mater Syst Struct* 1999;10:155.
- [16] Landis CM. *J Mech Phys Solids* 2002;50:127.
- [17] Hill R. *J Mech Phys Solids* 1967;15:79.
- [18] Huber JE, Fleck NA. Manuscript in preparation 2003.